Plasma Sources Sci. Technol. **18** (2009) 025019 (8pp) doi:10.1088/0963-0252/18/2/025019

Using a helicon source to simulate atmospheric re-entry plasma densities and temperatures in a laboratory setting

K M Lemmer, A D Gallimore and T B Smith

Department of Aerospace Engineering, University of Michigan, 1320 Beal Ave, Ann Arbor, MI 48019, USA

E-mail: klemmer@umich.edu

Received 19 November 2008, in final form 26 January 2009
Published 4 March 2009
Online at stacks.iop.org/PSST/18/025019

Abstract

The purpose of this research is to develop a plasma system capable of reproducing plasma densities found during atmospheric re-entry of a capsule. We developed a 150 mm diameter helicon source at the University of Michigan Plasmadynamics and Electric Propulsion Laboratory (PEPL) and used a Langmuir probe to characterize plasma properties downstream. The helicon source was operated with argon gas at a background pressure of 0.6 mTorr. We used a commercial RF-compensated single Langmuir probe to measure ion number density and electron temperature in the region downstream of the helicon source where we want to create conditions similar to those found during hypersonic flight within the atmosphere. We measured these values with and without the presence of a large 450 mm wide by 550 mm long surface downstream in the horizontal plane to simulate a vehicle surrounded by plasma in order to determine how the downstream body affects plasma properties. We found that the presence of a surface downstream of the helicon source lowers the downstream plasma density range from between 1.7×10^{17} and 3.3×10^{17} m^{-3} down to 0.55×10^{17} and 1.3×10^{17} m^{-3}. In addition, the peak plasma potential decreases from 65 to 55 V, but the electron temperature remains unchanged ranging between 1.5 and 6.5 eV.

1. Introduction

When a hypersonic vehicle travels through the atmosphere, a high-density, low-temperature plasma sheath forms around it. This plasma sheath prevents radio signals from passing through it causing communications blackout. This blackout first became an issue during the space race at the beginning of human spaceflight. The public became very aware of the problem while awaiting Apollo 13's return from blackout during their atmospheric re-entry from a failed moon landing attempt. When NASA began using the Space Shuttle for ferrying humans to and from space, and with the launch of the Tracking and Data Relay Satellite (TDRS) system, the communications blackout was no longer an issue for human spaceflight since the orbiter is not fully encapsulated in plasma during its re-entry, allowing radio signals to use satellites in orbit to reach ground stations. However, with the move to return to an Apollo-like re-entry vehicle, Orion and the continued use of capsules for sample return missions, the communications blackout will remain a problem. In addition, the US Military is interested in maintaining constant Global Positioning System (GPS) communication with vehicles traveling at hypersonic speeds within the atmosphere for guidance.

During the height of the space race, extensive experimental work was done to study atmospheric re-entry plasmas both in laboratories and around re-entry vehicles. While most of the laboratory work concentrated on simulating the thermal and chemical phenomena that occur near the surface of a re-entry vehicle for testing heat shields [1–4], not much work was done to simulate the actual plasma number densities present during atmospheric re-entry. The experiments done on re-entry vehicles consisted mostly of electrostatic probe and microwave interferometer tests and successfully measured plasma density and electron temperature as functions of altitude and distance away from the re-entry vehicle [5, 6]. More recently, complex computer

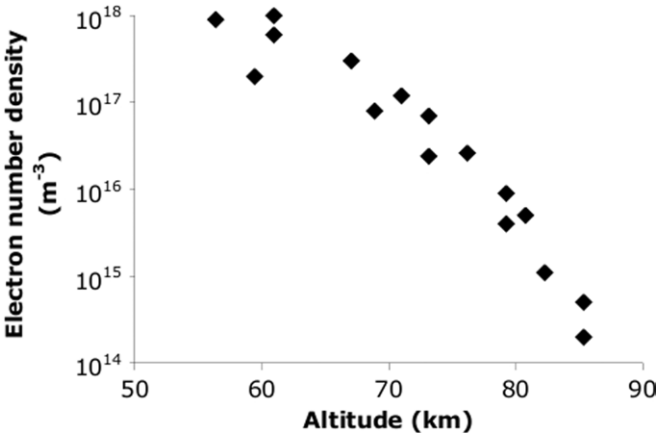

Figure 1. Electron number density as a function of altitude measured during RAM-C re-entry experiments [6].

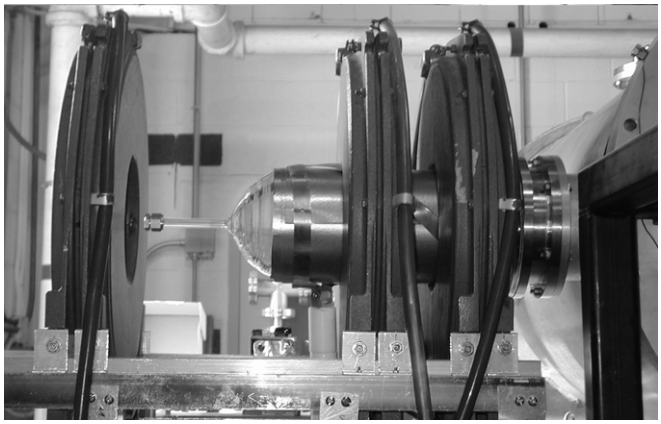

Figure 2. Helicon source shown attached to the Cathode Test Facility (CTF) at PEPL with one magnet pulled away to show antenna and quartz tube.

simulations have been developed to model the plasma that exists during atmospheric re-entry [7, 8].

The purpose of this research is to simulate re-entry plasma number densities found at various altitudes in a laboratory setting so that we can later manipulate the plasma to allow for continuous communications through the sheath [9]. In addition, we look at electron temperature and plasma potential. This research presents ion number density, electron temperature and plasma potential measurements downstream of a 150 mm diameter helicon source operating on argon at the Plasmadynamics and Electric Propulsion Laboratory (PEPL) at the University of Michigan (UM). These results were obtained with a single Langmuir probe (LP) located downstream of the helicon source. While inside the helicon source, the magnetic field reaches magnitudes up to 450 G, the peak magnetic fields experienced downstream by the LP in the region we probed are negligible. In addition, the probe is oriented perpendicular to the magnetic field, and thus, the magnetic field effects on probe current collection are minimized [10]. The measurements were taken in a 3D map in the region between 200 and 380 mm downstream of the source exit plane for two conditions: with only the LP downstream of the helicon source and with both the LP and a surface in the horizontal plane representing a hypersonic vehicle downstream of the helicon source. Data presented in this paper reflect three horizontal planes of the 3D map.

Ion number density and electron temperature data obtained are compared with those found in the 1970s during electrostatic probe testing on RAM-C re-entry capsules. During the re-entry experiments, electron number densities ranged from 10^{14} m^{-3} at an altitude of 85 km up to 10^{18} m^{-3} at an altitude of 56 km. Figure 1 shows how the electron number density varied as a function of altitude during the RAM-C re-entry experiments. Electron temperatures were found to range from 0.17 up to 1.3 eV [5, 6]. Since matching plasma number density is the main goal of this research, we are not concerned with whether the simulated plasma is flowing. In addition, re-entry plasma sheaths occur behind very strong shocks and within boundary layers, so the plasma does not flow at supersonic speeds close to the vehicle body [9].

2. Facilities and experimental setup

All testing was performed at PEPL in the Cathode Test Facility (CTF). The CTF is a 2.44 m long by 0.61 m diameter aluminum-walled vacuum chamber that also served as the ground reference for the duration of these experiments. An attached cryopump is able to pump the chamber down to a base pressure of 3×10^{-7} Torr and is able to maintain pressures up to 1 mTorr with gas flow. The helicon source is connected via a rubber O-ring to a 145 mm diameter port that is located on the side of the CTF. In addition, there are three high-precision linear tables inside the vacuum chamber that allow for complete three-dimensional LP mapping.

2.1. PEPL helicon source

The helicon source at PEPL consists of a 300 mm long double helix antenna wrapped around a 150 mm diameter by a 400 mm long quartz tube that is connected via a pi-style matching network to a 3 kW, 13.56 MHz RF power supply. The matching network limits the reflected power to 10% of the input power. The required 450 G magnetic field is provided by three electromagnets (figure 2) powered by a 60 A dc power supply. Argon flows into the CTF via a needle valve through a nozzle on the opposite end of the quartz tube so that the background pressure remains at 0.6 ± 0.05 mTorr. Argon gas is used to simulate the re-entry plasma because it ionizes much easier than air, and we are only trying to reproduce the plasma density, not the plasma composition.

Figure 3 shows the physical layout of the PEPL helicon source and downstream surface from two angles. The origin (0,0,0 position) refers to the radial centerline of the quartz tube in the axial location where the quartz tube meets an adapter flange. Testing was done with both an empty vacuum chamber downstream of the helicon source and with a blunt body representing the surface of a hypersonic vehicle downstream. The blunt body consists of a 450 mm wide by 550 mm long mica sheet perched atop a 320 mm diameter copper and iron cylindrical stand. The mica sheet is located immediately downstream of the exit plane of the helicon source in a vertical plane at the −70 mm position, as indicated in figure 3, so that

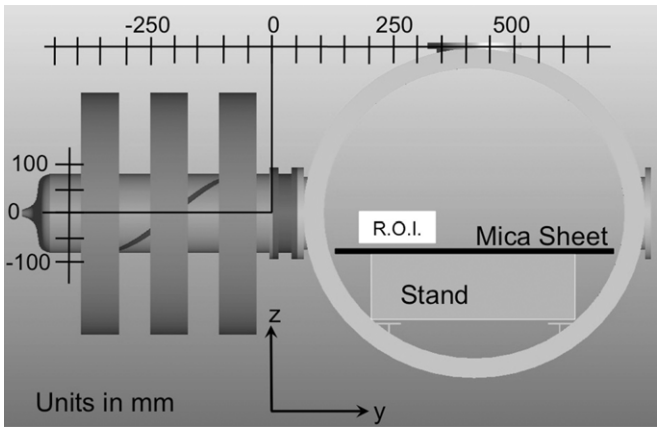

(a)

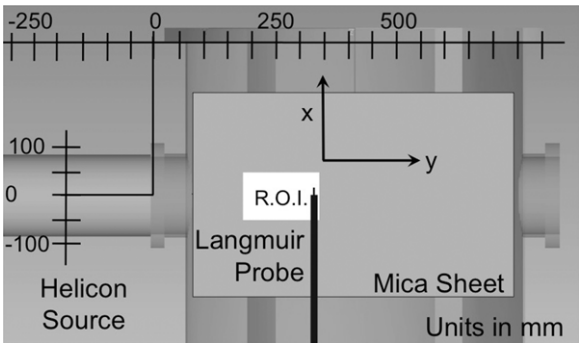

(b)

Figure 3. PEPL helicon layout shown from (*a*) the radial (x) direction and (*b*) looking down upon the mica surface from the vertical (z) direction. In both figures, the (0,0,0) measurement point is indicated along with the ROI where Langmuir probe data were obtained and the location of the mica sheet when present.

the plasma sheath is above the mica surface. Mica was chosen to simulate the hypersonic surface because it is a dielectric material with good electrical and thermal insulation. The region of interest (ROI) in this experiment is also indicated in figure 3 and ranges from −50 to 50 mm in the radial (x) direction, from 180 to 340 mm downstream of the origin in the axial (y) direction and from 0 to −60 mm in the vertical (z) direction.

2.2. *Langmuir probe*

All measurements were done with a commercial RF-compensated single LP system from the Hiden Corporation that consists of a data acquisition software package, a tungsten LP collector, RF compensation circuitry (LP blocking impedance is 4.25 MΩ at 13.56 MHz), a power supply and an ammeter. The software package communicates via a serial connection to the hardware box, which in turn provides the bias voltage to and reads a current from the LP collector. The LP has a single 1.78 mm long by 0.15 mm diameter tungsten collector.

Raw LP data are displayed and stored as current versus voltage sweeps (IV curves) at a resolution of about nine points per volt. For each downstream location, three IV curves were measured and smoothed using a 7-point box-smoothing spline built into the Hiden software package. We smooth the data to eliminate any 13.56 MHz noise that the lines may pick up

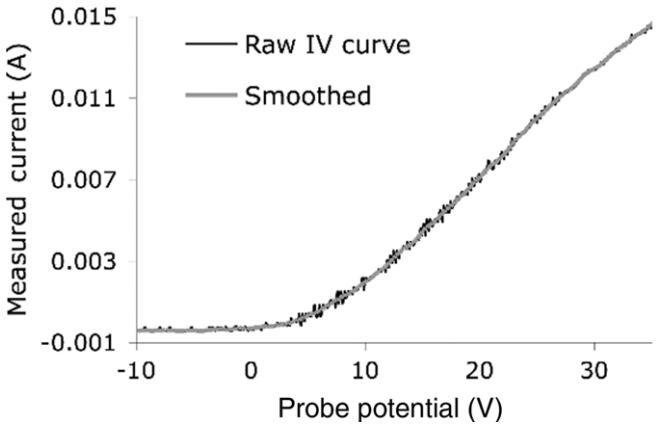

Figure 4. Measured raw IV curve and the corresponding smoothed IV curve.

during testing. This process step facilitates calculation of the ion number density and electron temperature from the IV curves. Figure 4 shows a representative example of the raw and corresponding smoothed IV curve for a single sweep.

After smoothing the IV curves, we analyzed the data using Matlab. First, we averaged the three traces and then found the floating potential as the voltage where the collected current is zero. Next, we calculated the ion number density based on the Orbital Motion Limited (OML) assumption using techniques developed by Laframboise [11, 12]. These techniques assume that a cylindrical probe is immersed in a cold, collisionless, stationary plasma, and that the plasma sheath dimensions increase as a function of the probe potential in such a way that the collected ion current is affected. The ion number density, n_i, is calculated using (1)

$$n_i = \frac{1}{A_p}\sqrt{\frac{2\pi M_i}{1.27e^3}\left(\frac{dI_i^2}{dV}\right)}, \tag{1}$$

where A_p is the LP collector surface area, M_i is the ion mass of argon, e is the elementary charge, I_i is the ion probe current and V is the probe bias voltage.

We determined that the LP was operating in the OML regime by finding that the probe radius-to-Debye length ratio is less than three, where the Debye length, λ_D, is found using (2) [13].

$$\lambda_D = \sqrt{\frac{k_B T_e}{4\pi n_e e^2}}. \tag{2}$$

where k_B is Boltzmann's constant, T_e is the electron temperature in eV and n_e is the electron number density. For our case, we assume that the plasma is quasi-neutral, so that the ion number density and the electron number density are equal.

Electron temperature is calculated using the inverse slope of the natural log of the electron current versus the probe potential in the region of electron current collection [10]. We assume the electron energy distribution function is Maxwellian based on previous experiments done on helicon sources with operating conditions similar to those found in our

experiment [14].

$$T_e(\text{eV}) = \frac{V_2 - V_1}{\ln\left(\frac{I_2}{I_1}\right)}. \quad (3)$$

Finally, we found the plasma potential using the electron temperature (in eV), floating potential (V_f), the ion mass and the electron mass (m_e). We could not get plasma potential directly from the IV curves because the ammeter built into the Hiden system saturated prior to entering the electron saturation regime.

$$V_p - V_f = \ln\left(\sqrt{\frac{M_i}{m_e}}\right) T_e. \quad (4)$$

We use traditional LP error estimates of 20% for electron temperature and 50% for ion number density in our experiment [10]. Although these errors are high when looking at absolute values for electron temperature and ion number density, we can still effectively study trends that occur within the plasma as the relative error between measurements using the same experimental apparatus is considerably lower [15]. We did not have to take magnetic field effects into account since the area of interest is far enough downstream such that the helicon magnetic field is small (<5 G), resulting in an ion gyroradius that is much much larger than the probe diameter [10].

3. Results and discussion

First, we wanted to confirm that the plasma source was operating in helicon mode. Then, we found results for ion number density in the region downstream of the helicon source and compared them with those found during the RAM-C experiments. In addition, we found electron temperature and plasma potential for the same region. During helicon mode operation, we found that in general the ion number density, electron temperature and plasma potential decrease with increasing y-position. This trend is more evident along the $z = 0$ plane than in the lower z-planes. In addition, when a body is present downstream, the overall ion number density and the peak plasma potential decrease; however, the electron temperature remains independent of the presence of a downstream body. Our experiments were conducted with an argon chamber pressure of $0.6 \pm .05$ mTorr. These conditions result in an ion–neutral mean free path on the order of meters [21], which is much larger than the region of investigation.

3.1. Helicon mode operation

We verified that we were operating in helicon mode for the conditions that we used in these experiments: input power = 1500 W, magnetic field strength = 450 G peak centerline in the y-direction and downstream pressure = 1 mTorr. LP tests were conducted inside the quartz tube at the $y = -100$ mm position and at the centerline of the helicon source ($z = 0$ mm). LP data were analyzed using a combination of thin sheath and OML methods to find ion number density. This method for LP analysis is explained in detail in [16]. During these tests, we varied the input power, dc magnetic field strength and LP position in the x direction. Figure 5(a) shows the three 'density jumps' that are consistent with the capacitive, inductive and helicon modes of operation [17]. These 'jumps' become obvious at a peak axial magnetic field (B_y) of 290 G, and are even more prominent at 440 G. Figure 5(b) shows the density peak at the center ($x = 0$) of the quartz tube with higher input power, indicating helicon mode operation. Also shown is the 'volcano-like' structure of the radial density profile at lower input power consistent with capacitive and inductive modes [18–20]. For all input power levels presented in figure 5(b), the peak centerline dc magnetic field is 440 G in the y-direction.

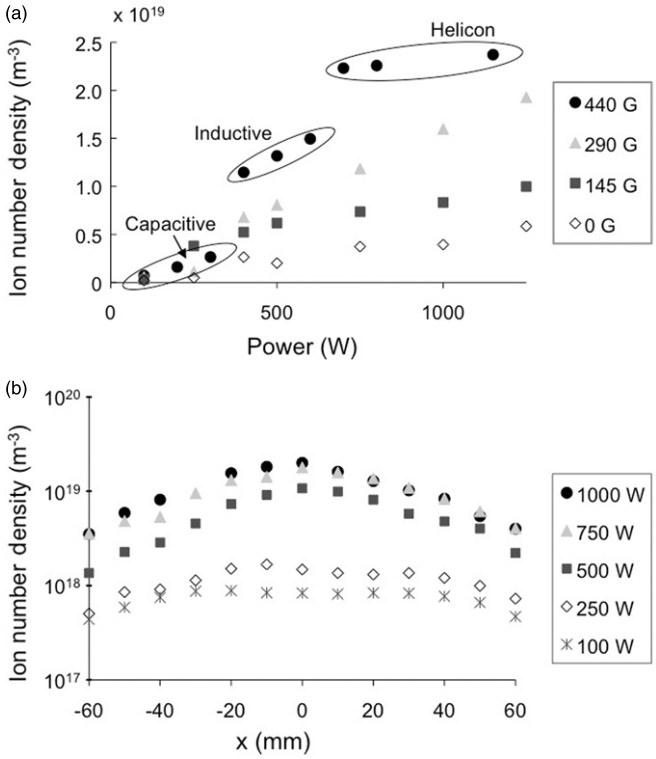

Figure 5. Verification of helicon mode operation of the PEPL helicon source while operating with argon at a background pressure of 0.6 mTorr at the $y = -100$ mm position. (a) Ion number density measurements inside the helicon source for varying input power and magnetic field. (b) Ion number density measurements as a function of x-position and input power for 440 G peak magnetic field strength in the y-direction.

3.2. Ion number density

We first wanted to characterize the plasma downstream of the helicon source with no body present. Figure 6 shows the ion number density as a function of x- and y-positions for three planes along the z-axis: the helicon centerline ($z = 0$ mm) and 30 and 60 mm below the helicon centerline. With no body present, we found ion number densities ranging from 1.5×10^{17} to 3.3×10^{17} m^{-3}. These number density values are representative of re-entry plasma densities found at altitudes ranging from 60 to 70 km (figure 1). The highest densities are found nearest to the helicon source exit plane at the $z = 0$ position in the positive x-region (figure 6(a)). The higher densities in the positive x-region are expected due to the nature of the experimental setup. There is a flange in the

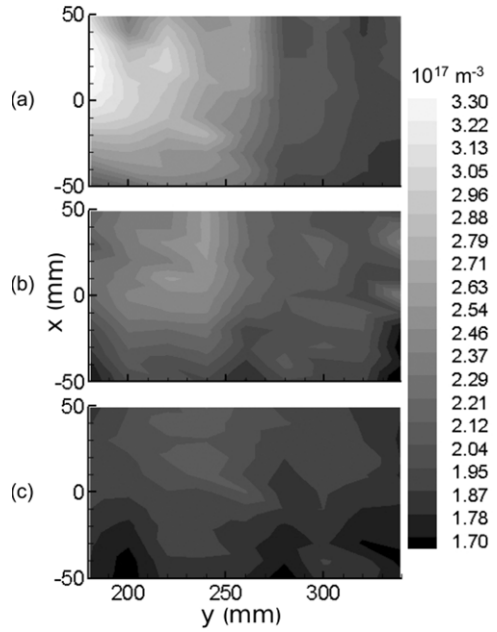

Figure 6. Ion number density as a function of x and y LP position with an empty chamber downstream for (a) $z = 0$ mm, (b) $z = -30$ mm and (c) $z = -60$ mm

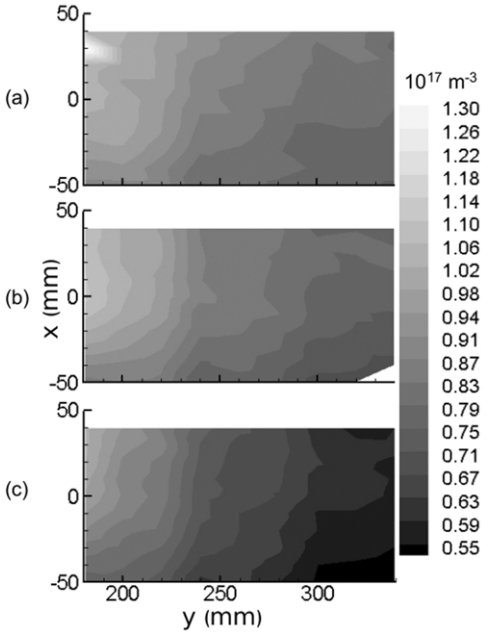

Figure 7. Ion number density as a function of x and y LP position with a body downstream of the helicon source simulating a 'vehicle surface' for (a) $z = 0$ mm, (b) $z = -30$ mm and (c) $z = -60$ mm.

plane along $x = 305$ mm and empty chamber in the negative x-direction, as is shown in figure 3(b). In addition, we see from the density maps that while at $z = 0$ (figure 6(a)), the ion number density decreases with increasing y-position, in the lower z-planes (figures 6(b) and (c)) the ion number density becomes independent of the downstream y-location.

Next, we looked at how the addition of a body for simulating a vehicle surface downstream of the helicon source affected the ion number density. We found that the addition of the body decreased the ion number density by a factor of 2.5. Figure 7 shows the ion number densities downstream of the helicon source at the same three z-positions as in figure 6. In addition, figure 8 is added for clarity. It shows the ion number density as a function of the y-position for the same z-positions as figures 6 and 7 along the x-axis for both the empty chamber case and the case with a body downstream. Similar to the case with an empty chamber downstream, the ion number density is highest nearest the helicon exit plane, at $z = 0$ in the positive x-region (figure 7(a)). The addition of a body downstream, though, causes the ion number density to be dependent on the y-position for all z-planes. The density range found with a body present downstream of the helicon source (5.0×10^{16} to 1.3×10^{17} m^{-3}) is representative of that found at altitudes from 65 to 75 km during atmospheric re-entry (figure 1).

3.3. Electron temperature

Electron temperature ranged from 2 to 6.5 eV for the ROI in these experiments. Although these values are similar to what we expected based on previous experiments done inside and immediately downstream of helicon sources [22], they are higher than those measured during the RAM-C experiments mentioned in section 1. This temperature difference (in some cases as high as 6 eV) is acceptable since number density

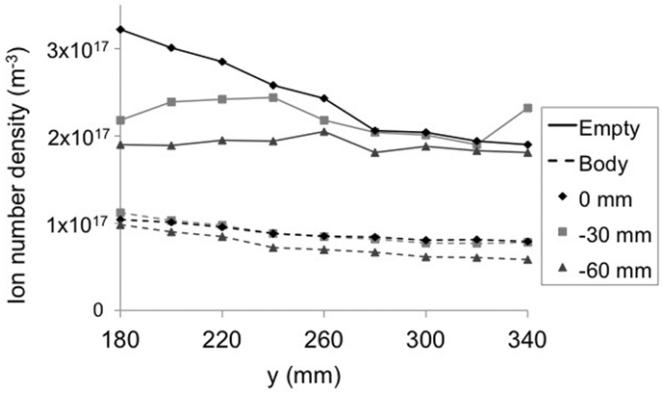

Figure 8. Ion number density as a function of y-position with an empty chamber downstream of the helicon source and a body downstream of the helicon source simulating a 'vehicle surface' for three z-positions along the x-axis.

matching is the primary concern of this research, and we simply wanted to ensure that the electron temperature was of a similar order of magnitude to that found during atmospheric re-entry.

Figures 9–11 show the electron temperature in the same locations and for the same conditions as figures 6–8, respectively. While the electron temperature is, in general, not strongly correlated with downstream position, there does appear to be a warm core along the z-axis (figure 9(a)) when the chamber is empty downstream of the helicon exit plane. The plasma cools as we move away from the z-axis. Also, the presence of a body downstream of the helicon source eliminates this warm core.

3.4. Plasma potential

Figures 12–14 show the plasma potential as a function of x and y downstream positions for the same three z-planes show

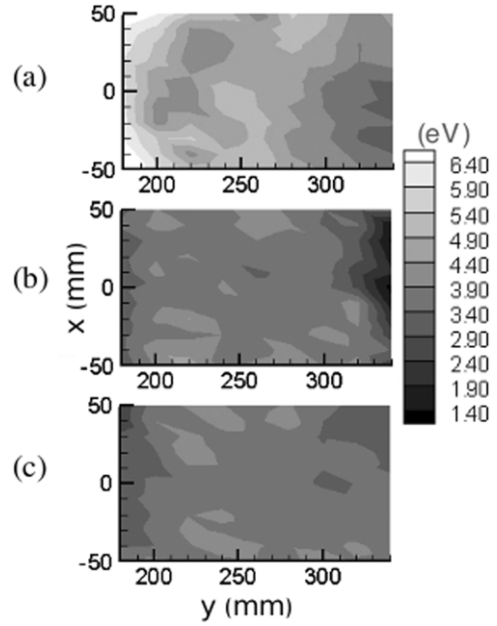

Figure 9. Electron temperature as a function of x and y LP position with an empty chamber downstream for (a) $z = 0$ mm, (b) $z = -30$ mm and (c) $z = -60$ mm

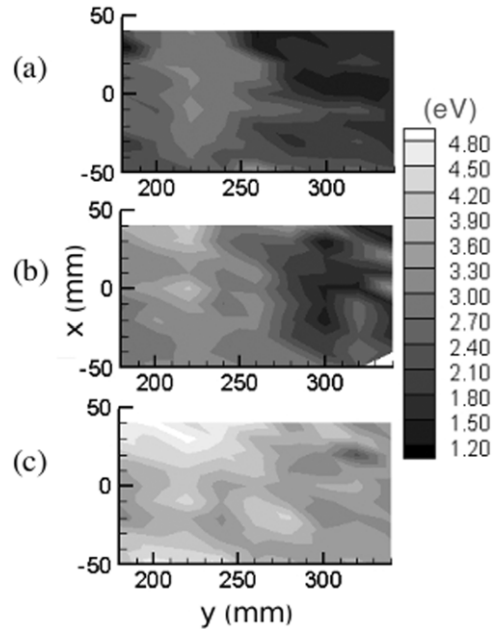

Figure 10. Electron temperature as a function of x and y LP position with a body downstream of the helicon source simulating a 'vehicle surface' for (a) $z = 0$ mm, (b) $z = -30$ mm and (c) $z = -60$ mm.

previously: $z = 0$ mm, $z = -30$ mm and $z = -60$ mm. We found that, in general, the plasma potential is lower further downstream of the helicon source. The decrease in plasma potential is not consistent with what is expected from the Boltzmann relation [23], which suggests that the plasma potential should be related to the number density by equation (5):

$$n = n_{\mathrm{o}} \exp\left(\frac{eV_{\mathrm{p}}}{kT_{\mathrm{e}}}\right), \tag{5}$$

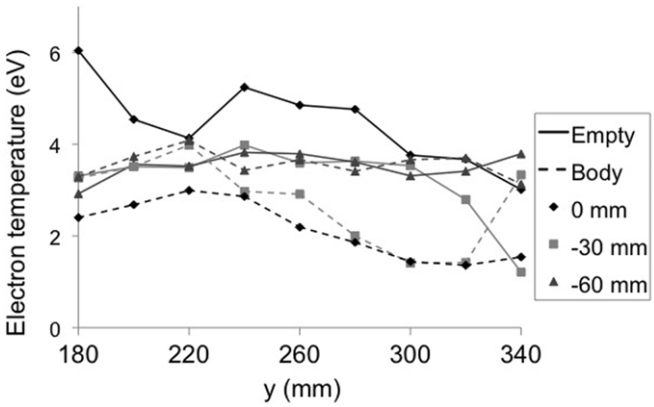

Figure 11. Electron temperature as a function of y-position with an empty chamber downstream of the helicon source and a body downstream of the helicon source simulating a 'vehicle surface' for three z-positions along the x-axis.

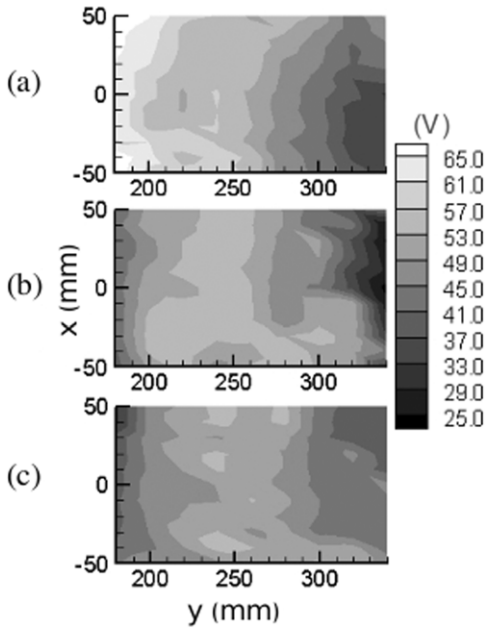

Figure 12. Plasma potential as a function of x and y LP position with an empty chamber downstream for (a) $z = 0$ mm, (b) $z = -30$ mm and (c) $z = -60$ mm.

where n and n_{o} are the number density and reference number density, respectively and T_{e} is in Kelvin. If the Boltzmann relation were applied to the measured number density and plasma potential, the electron temperature would be around 60 eV.

4. Conclusions

We found ion number densities ranging from 1.7×10^{17} to 3.3×10^{17} m^{-3} with an empty chamber downstream of the helicon source and from 0.5×10^{17} to 1.3×10^{17} m^{-3} with a body downstream of the helicon source to simulate a re-entry vehicle. Ion number densities are higher, in general, closer to the helicon source exit ($y = 0$ mm) and centerline ($z = 0$ mm). Electron temperatures ranged from 2 to 6.5 eV with the only

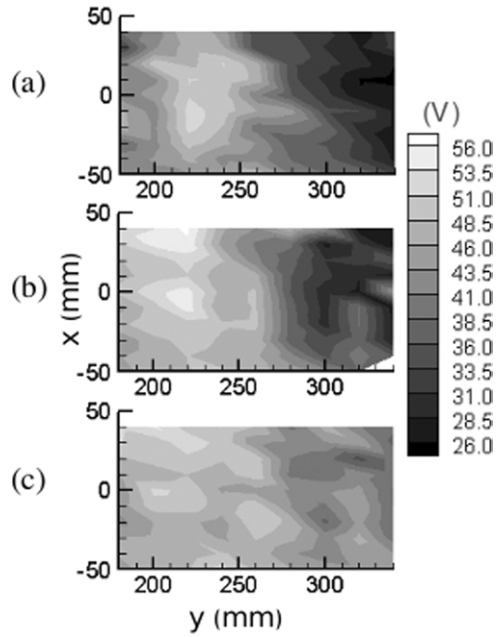

Figure 13. Plasma potential as a function of x and y LP position with a body downstream of the helicon source simulating a 'vehicle surface' for (a) $z = 0$ mm, (b) $z = -30$ mm and (c) $z = -60$ mm.

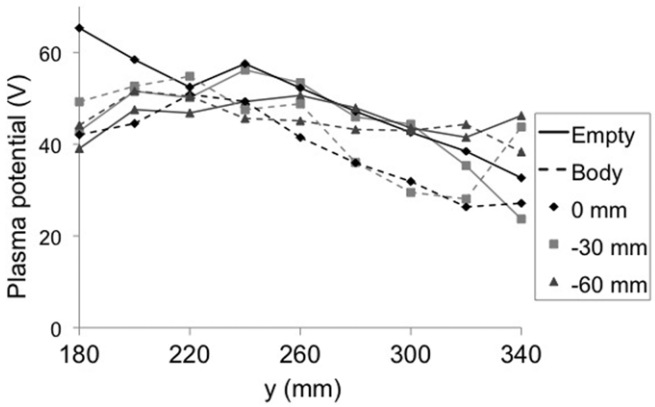

Figure 14. Plasma potential as a function of y-position with an empty chamber downstream of the helicon source and a body downstream of the helicon source simulating a 'vehicle surface' for three z-positions along the x-axis.

discernible difference coming from the cooling of the plasma along the z-axis with the addition of a body downstream. The plasma potential ranged from 25 to 65 V with peak values occurring when no body is present downstream. The plasma potential is also not strongly correlated with the downstream position.

Since the goal of this research is to show that our helicon source can be used to simulate the plasma densities found during atmospheric re-entry, we compared the data we found during our investigation with those obtained in the RAM-C re-entry experiments. The RAM-C experiments show re-entry electron number densities ranging from $10^{14}\,\mathrm{m}^{-3}$ for higher altitudes (85 km) to $10^{18}\,\mathrm{m}^{-3}$ for lower altitudes (56 km) [5, 6]. We assume a quasi-neutral plasma, so comparing the ion number densities found during our experiments with those found during the RAM-C experiments show that we are simulating the density of the re-entry plasma sheath that occurs at altitudes ranging from 60 to 75 km.

References

[1] Rybak J P and Churchill R J 1971 Progress in reentry communications *IEEE Trans. Aerospace Electron. Syst.* **AES-7** 879–94
[2] Lukasiewicz J, Whitfield J D and Jackson R 1962 Hypersonic flow research *Prog. Astronaut. Rocketry* **8** 473–511
[3] Winovich W and Carlson W C A 1979 The 60 mw shuttle interaction heating facility *Proc. 25th Int. Instrumentation Symp. (Anaheim, CA)*
[4] Auweter-Kurtz M, Kurtz H L and Laure S 1996 Plasma generators for re-entry simulation *J. Propulsion Power* **12**
[5] Grantham W L 1970 Flight results of a 25 000-foot-per-second reentry experiment using microwave reflectometers to measure plasma electron density and standoff distance *NASA Technical Note* D-6062, Langley Research Center, Hampton, VA
[6] Jones W L Jr and Cross A E 1972 Electrostatic probe measurements of plasma parameters for two reentry flight experiments at 25 000-feet-per-second *NASA Technical Note* D-6617 Langley Research Center, Hampton, VA
[7] Scalabrin L C and Boyd I D 2006 Numerical simulation of weakly ionized hypersonic flow for reentry configurations *AIAA Paper* 2006-3773
[8] Costa R R, Silva J S, Wu S F, Chu Q P and Mulder J A 2002 Atmospheric reentry modeling and simulation *J. Spacecraft Rockets* **39** 636–9
[9] M Keidar, Km M and Boyd I D 2008 Electromagnetic reduction of plasma density during atmospheric reentry and hypersonic flights *J. Spacecraft Rockets* **45** 445–53
[10] Hutchinson I H 2002 *Principles of Plasma Diagnostics* 2nd edn (Cambridge: Cambridge University Press)
[11] Laframboise J G and Parker L W 1973 Probe design for the orbit-limited current collection *J. Fluids* **6** 629–36
[12] Laframboise J G and Rubinstein J 1976 Theory of a cylindrical probe in a collisionless magnetoplasma *J. Fluids* **19** 1900–8
[13] Chen F F 1965 *Plasma Diagnostic Techniques, Electric Probes* (New York: Academic)
[14] Takahasi K, Charles C, Boswell R W, Kaneko T and Hatakeyama R 2007 Electron dynamics in a current-free helicon double layer *The 9th Int. Workshop on the Interrelationship between Plasma Experiments in Laboratory and Space (Cairns, Australia)* (Piscataway, NJ: IEEE)
[15] Foster J E 2002 Intercusp electron transport in an nstar-derivative ion thruster *J. Propulsion Power* **18** 213–7
[16] Linnell J A 2007 An evaluation of krypton propellant in hall thrusters *PhD Thesis* University of Michigan
[17] Boswell R W 1974 A study of waves in gaseous plasmas *PhD Thesis* Flinders University of South Australia
[18] Chen F F and Boswell R W 1997 Helicons—the past decade *IEEE Trans. Plasma Sci.* **25** 1245–57
[19] Kitajima T, Izawa M, Nakano N and Makabe T 1997 The time-resolved two-dimensional profile of a radiofrequency capacitively coupled plasma *J. Phys. D: Appl. Phys.* **30** 1783–989
[20] Ventzek P L G, Sommerer T J, Hoekstra R J and Kushner M J 1993 Two-dimensional hybrid model of inductively coupled plasma sources for etching *Appl. Phys. Lett.* **63** 605–7

[21] Roth J R 2001 *Industrial Plasma Engineering Volume 2: Applications to Nonthermal Plasma Processing* (London: Institute of Physics)

[22] Porte L, Yun S M, Arnush D and Chen F F 2003 Superiority of half-wavelength helicon antennae *Plasma Sources Sci. Technol.* **12** 287–93

[23] Chen F F 1984 *Introduction to Plasma Physics and Controlled Fusion Volume 1: Plasma Physics* (New York: Plenum) 2nd edn

[24] Charles C and Boswell R 2003 Current-free double-layer formation in a high-density helicon discharge *Appl. Phys. Lett.* **82** 1356–8